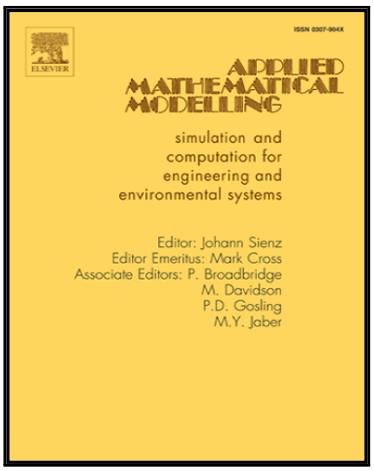

Bending and Twisting Friction Models in Soft-Sphere Discrete Element Simulations for Static and Dynamic Problems

M.A.J. Holmes , R. Brown , P.A.L. Wauters , N.P. Lavery , S.G.R. Brown

PII: S0307-904X(15)00688-5
DOI: 10.1016/j.apm.2015.10.026
Reference: APM 10838

To appear in: *Applied Mathematical Modelling*

Received date: 2 April 2015
Revised date: 14 October 2015
Accepted date: 19 October 2015

Please cite this article as: M.A.J. Holmes , R. Brown , P.A.L. Wauters , N.P. Lavery , S.G.R. Brown , Bending and Twisting Friction Models in Soft-Sphere Discrete Element Simulations for Static and Dynamic Problems, *Applied Mathematical Modelling* (2015), doi: 10.1016/j.apm.2015.10.026

Highlights

- DEM model with shear, rolling (bending and twisting) frictional forces is presented
- Improved predictions obtained for a modified bending friction formulation
- Effects of bending/twisting in static and dynamic test cases are demonstrated
- Effects of dampening in static and dynamic test cases are demonstrated

Bending and Twisting Friction Models in Soft-Sphere Discrete Element Simulations for Static and Dynamic Problems

M.A.J. Holmes[1], R. Brown[2], P.A.L. Wauters[2], N.P. Lavery[1], S.G.R. Brown[1]*

[1]Materials Research Centre
College of Engineering
Swansea University Bay Campus
Fabian Way
Swansea
Neath Port Talbot
SA1 8QQ
UK

[2] Tata Steel UK Ltd
Port Talbot Works
Port Talbot
South Wales
SA13 2NG
UK

*corresponding author s.g.r.brown@swansea.ac.uk

Abstract

In soft-sphere discrete element models of granular flow, particles may interact in a variety of ways including interactions normal to points of contact and interactions tangential to points of contact such as sliding, rolling, bending and twisting. In the majority of models normal and sliding modes are used. Rolling friction is sometimes reported but incorporation of bending and twisting effects is less common. In this paper it is shown that the precise mathematical nature of bending and twisting models in soft-sphere simulations can have significant effects on model predictions, especially for the case of dynamic granular flow problems.

Keywords: Discrete Element Simulation, Bending, Twisting, Friction.

Introduction

This paper arises out of industrial research concerning the development of new material distribution prediction methods for the Port Talbot Works of TATA steel. The industrial focus of the work is a better understanding of the charging of raw material (e.g. coke, iron ore and sinter) collectively known as ‘burden’ into blast furnaces [1]. Kurunov identified that burden charging in the blast furnace affects furnace productivity and that the choice of charging system can improve furnace productivity by up to 7% and reduce coke usage by up to 7.6% [2]. However, to do so requires an understanding of dynamic 3D loading patterns.

The blast furnace is a hostile environment which makes in-process monitoring extremely difficult. Realistic simulation of the dynamic granular flows within the

blast furnace is therefore highly desirable. Discrete Element Method (DEM) has been used by several researchers to model blast furnaces although these models often assume radial symmetry and are not true scale simulations [3-5]. While true scale simulation has been reported [1] the details of the tangential interactions between particles can have a significant effect on model predictions. This is especially true for the largely dynamic case of blast furnace charging where continuous granular flow of material is important rather than the simpler case of static pile formation of granular materials. This prompted the investigation described here. In this paper the effects of tangential forces in soft-sphere DEM models are specifically investigated for two test cases. The case of static pile build up in a previously reported 'ledge test' example is considered first. Then a second dynamic case of a rotating drum containing granular material is investigated.

This paper limits itself to descriptions of the common frictional models used in DEM simulations. The usual differentiations between various types of friction are used namely shear and rolling, where rolling can be decomposed into bending and twisting (where some authors refer to twisting as torsion).

Shear Friction

Sliding friction, F_s, is handled using the widely used linear damped spring in series with a sliding friction element which can be summarised as

$$F_s = \min\left(k_s \delta_s + \nu_s \dot{s}, \mu_s |F_n| \right) - \hat{s} \quad \ldots(1)$$

$$F_n = k_n \delta \hat{n} \quad \ldots(2)$$

$$\nu_s = 2\sqrt{K_s \frac{m_i m_j}{m_i + m_j}} - \frac{\log(1/\eta_n)}{\sqrt{\pi^2 + \log(1/\eta_n)^2}} \quad \ldots(3)$$

where F_n is the normal contact force, k_n is spring strength, δ is overlap between spheres, $\hat{n}$ is the direction of the normal, μ_s is the coefficient of sliding resistance, k_s is a spring stiffness, δ_s is a contact overlap, ν_s is a dampening term, η_n is the coefficient of restitution, m is the mass of a particle, $\hat{s}$ is the surface tangent vector and $\dot{s}$ is relative velocity between a particle and another particle or object [6]. Here the tangential stiffness is constant for the no-slip condition, shear tractions are singular at the edges of the contact region, and there is a non-linear stiffness for a constant normal load and a monotonically increasing tangential load.

Rolling Friction

Rolling friction is a resistive force that slows down the motion of a rolling particle and is typically a combination of several frictional forces at the point of contact between the rolling particle and another particle or surface. In reported DEM models there are several ways of incorporating rolling friction effects. Zhou et al [7] describe conventional treatments of rolling friction where the friction may be either (i) independent of the angular velocity or (ii) directly proportional to the relative angular velocity of two particles in contact.

Case (i): Direction-constant torque model

The direction of the rolling frictional torque always opposes the relative rotation and is proportional to the normal contact force. This is a typical direction-constant torque model. In a 2D for model (i) the torque between two contacting discs, i and j, can be expressed using a normalised relative angular velocity as

$$T_r = -\frac{\omega_{rel}}{|\omega_{rel}|}\mu_r R_r F_n \quad \ldots(4)$$

$$\omega_{rel} = \omega_i - \omega_j \quad \ldots(5)$$

where μ_r is the coefficient of rolling resistance, ω_i and ω_j are the angular velocities of disks i and j respectively, ω_{rel} is the relative angular velocity between them and R_r is the so-called 'rolling radius' given by

$$R_r = r_i r_j / (r_i + r_j) \quad \ldots(6)$$

where r_i and r_j are the radii of contacting particles i and j.

Case (ii): Viscous model

Rolling frictional torque is proportional to the relative translational velocity arising from the relative angular velocity at a contact point between two particles as

$$T_r = -\mu_r R_r F_n (\omega_i r_i - \omega_j r_j) \quad \ldots(7)$$

This is a typical viscous model. 3D numerical results on sand pile simulations showed that treatment (i) gave better results than treatment (ii). Zhou et al [8] subsequently assessed this methodology by comparing to experimental data for mono-sized spheres. Combinations of approaches (i) and (ii) have also been used [9] where the rolling frictional torque contains both viscous and slider effects represented as,

$$T_r = \min(-\mu_r |F_n|, -\mu_r |\omega_{rel}|)\left(\frac{\omega_{rel}}{|\omega_{rel}|}\right) \quad \ldots(8)$$

where ω_{rel} is the vector of the relative tangential rotation of particles i and j.

Approaches (i) and (ii) above, plus a third approach (case (iii) below) using an elastic-plastic spring-dashpot model, were assessed in 2D by Ai et al [10].

Case (iii): Elastic-plastic spring-dashpot

In an elastic-plastic spring-dashpot method two contributions to the total resistance torque T_r are defined, a spring torque T^k_r and a viscous damping torque T^d_r expressed as

$$T_r = T_r^k + T_r^d \quad \ldots(9)$$

The viscous damping torque, T^d_r, depends on the rolling angular velocity between two particles in contact and a viscous damping coefficient. Full details are available in [10], in this formulation it is possible to adjust both when, and to what level, the viscous damping term is active. To calculate spring displacement for shear, rolling and twisting for non-deforming particles the displacements must be tracked. This integration is done using a Taylor expansion (δ_r is displacement, $F_{r,i}$ is the force due to rolling resistance and $T_{r,j}$ is the torque). ν_r is the dampening term, η_r is the dampening ratio,

Relative bending: $$V_{r\,\omega,ij} = \left(\omega_i \times r_i\right) - \left(\omega_j \times r_j\right) \quad \ldots(10)$$

$$\delta_r = \left(V_{r\,\omega,ij,\Delta t}\, dt\right) + \left(\dot{V}_{r\,\omega,ij,\Delta t}\, \frac{dt^2}{2}\right) + \left(\dot{V}_{r\,\omega,ij,\Delta t} - \dot{V}_{r\,\omega,ij,\Delta t-1}\, \frac{dt^2}{6}\right) \quad \ldots(11)$$

$$\nu_r = \eta_r 2 \sqrt{\frac{1}{\frac{1}{\left(1.4 m_i r_i^2\right)} + \frac{1}{\left(1.4 m_j r_j^2\right)}} K_s} \quad \ldots(12)$$

$$F_{r,i} = -\min\left(k_s \delta_r + \nu_r V_{r\,\omega,ij}\ ,\ \mu_r R_r |F_n| \frac{V_{r\,\omega,ij}}{|V_{r\,\omega,ij}|}\right) \quad \ldots(13)$$

$$T_{r,i} = r_i \times F_{r,i} \quad \ldots(14)$$

$$\therefore T_{r,j} = r_j \times -F_{r,i} \quad \ldots(15)$$

$$if\ slider\ activated\ \delta_r = \frac{\mu_r R_r |F_n| \hat{n}}{k_r} \quad \ldots(16)$$

Decomposing Rolling into Bending and Twisting Friction

Rolling forces can be decomposed into bending and twisting components. Using a bending term alone can lead to a situation where rotational frictions are not captured (i.e. a particle on a horizontal wall that is rotating around the vertical axis will effectively rotate forever). Wang points out that when decomposing rotations into bending, decomposition of remaining rotations into twisting is a requirement [11]. Twisting is the application of direct torque along the normal axis. The following implementation is an "Elastic-plastic spring-dashpot model" with velocity and displacement being calculated from the rotations around the normal axis [12].

$$\omega_{ij} = \omega_i - \omega_j \quad \ldots(17)$$

$$\omega_t = \left(\omega_{ij} \cdot \hat{n}\right)\hat{n} \quad \ldots(18)$$

$$\delta_t = \left(\omega_{t,\Delta t}\, dt\right) + \left(\dot{\omega}_{t,\Delta t}\, \frac{dt^2}{2}\right) + \left(\dot{\omega}_{t,\Delta t} - \dot{\omega}_{t,\Delta t-1}\, \frac{dt^2}{6}\right) \quad \ldots(19)$$

$$T_{t,i} = -min\left(k_s \delta_t + \nu_r \omega_t\ , \mu_t R_r |F_n| \frac{\omega_t}{|\omega_t|}\right) \quad \ldots(20)$$

$$if\ slider\ activated\ \delta_t = \frac{\mu_t R_r |F_n| \frac{\omega_t}{|\omega_t|}}{k_t} \quad \ldots(21)$$

$$\therefore\ T_{t,j} = -T_{t,i} \quad \ldots(22)$$

Methods

An in-house soft-sphere DEM code written in FORTRAN90 has been used with 3D visualisation output obtained using the open source code ParaView, (www.paraview.org). In all simulations below there are no global dampeners and no numerical limiters.

Relative versus Summed rotational velocities for bending forces

In the case above the relative speed of rotation $\left(\omega_i \times r_i - \omega_j \times r_j\right)$ of the interacting particles is used to calculate the bending frictional force (this is designated as RSR). Khan and Bushell point out that using the relative speed of rotation at the surface is incorrect because, for the case of two particles with matching rotational speeds, the relative bending force will be zero when it should actually be at its highest [13]. Here we hypothesise that by separating rolling into bending and twisting, and then by using the summed speed of rotation $\left(\omega_i \times r_i + \omega_j \times r_j\right)$ for the bending resistance a better model of material behaviour is obtained (this is designated as SSR) shown in Figure 1a, b and c.

Summed bending: $$V_{r\,\omega,ij} = \left(\omega_i \times r_i\right) + \left(\omega_j \times r_j\right) \quad \ldots(23)$$

$$\therefore T_{r,j} = r_j \times F_{r,i} \quad \ldots(24)$$

Returning and non-returning dampeners

The effects of dampening are also investigated. In the normal contact force model a damped linear spring consists of two parts; the spring and the dampener [14]. If the dampener is applied in both direction of a collision (particles moving towards each other and particles moving apart) this is referred to here as returning dampening (RD). Dampening forces are used to represent the loss of energy during a collision (due to breakage, noise, heat etc.), they can cause the spring to reach equilibrium and they have the benefit of minimising numerical round-off and other integration problems. RD results in a negative force being applied directly in the normal direction as particles move apart, i.e. a compressive force. Compressive force is not part of the collision between dry non-sticky granular materials because there is no cohesive force and the material is in a state of elastic recovery. Applying a dampening force as particles move apart is not necessary in the industrial cases of interest to us. For comparison, in this paper we investigate both RD and non-returning dampening (NRD) where the latter case only applies dampening as particles move towards each other.

$$\dot{V}_{ij,n} = \left(V_{ij} \cdot \hat{n}\right) \quad \ldots(25)$$

Returning dampener (RD) $F_{dn} = v_n \dot{V}_{ij,n} \hat{n}$ …(26)

Non-returning dampener (NRD) $F_{dn} = max(v_n \dot{V}_{ij,n}, 0)\hat{n}$ …(27)

Figure 1d shows the difference between the RD and NRD models. A summary of the force model, including bending and twisting, is shown in figure 2. Simulation parameters and related information is given in Table 1. Initial trials on numerical test problems with a small number of mono-size spheres were conducted as verification tests of the models, these results are described in detail elsewhere [15].

Results and discussion

Figure 3 shows the results of simulations carried out using the test case devised by Zhou et al [7], referred to in this paper as the 'ledge test'. A static bed of particles is placed on a horizontal ledge. The left and right hand sections of this ledge are removed and particles at the edges fall down into the lower part of the chamber forming a pile with a depression at the centre. At the same time another static pile forms on the portion of the ledge which was not moved. In figure 3 (a) and (b) SSR has been used to calculate bending friction, with and without twisting. In contrast in figure 3 (c) and (d) the standard RSR approach has been used, again with and without the inclusion of twisting. In figure 3 an NRD model has been used in all cases. From the results it can be seen that higher angles of repose are obtained when the SSR is used to calculate bending friction. The inclusion or not of twisting has had a lesser, second order effect on the results. In this test case, the relatively small depth of the test means that the particle-sidewall friction effects contribute a large proportion of the overall frictional effects. Figure 4 shows the same four simulations but in all of these cases the RD model has been used instead. Again, the use of SSR has resulted in higher angles of repose and again the inclusion or not of twisting is a second order effect.

Too much emphasis should not be placed on these results. The use of SSR (with the same bending friction coefficient as used in RSR) would be expected to result in larger effective frictional forces and the trend of the results obtained. Figure 4 (e) shows the SSR/RD case (including twisting) again, but where this time the rolling and twisting coefficients have been halved. This result is much more similar to figures 3 (c) and (d) showing that SSR can provide the same result as RSR merely by changing friction coefficients. Figure 4 (e) is very similar to the results published in Zhou et al [7].

More dramatic results are shown in figures 5, 6, 7 and 8 in the 'drum test'. In these cases a rotating drum (with radius R = 0.1485 m) with a smooth internal surface is rotated at two different speeds. The drum is closed at both edges by sidewalls (not shown in the figures) and the increased depth of the simulation means that the overall proportion of particle-sidewall friction is reduced. The drum rotates anti-clockwise in all cases. Two drum rotational speeds have been investigated. The speed of rotation of the drum has been set at (i) less than the critical speed in some cases and (ii) greater than the critical speed in others. The critical speed of rotation (rpm) is calculated from the standard equation

$$Critical\ Speed = \frac{1}{2\pi}\sqrt{\left(g/(R-r)\right)} \quad \ldots(28)$$

Where R is the radius of the drum and r is particle radius. In figure 5 the SSR simulations show a marked difference in behaviour compared to the RSR cases for the case where the speed of rotation of the drum is 60 rpm (or 70% of the critical speed). Particles are lifted higher up the wall and there is much less rotational velocity (W) evident. In the RSR cases the particles remain near the bottom of the drum and have much higher rotational velocities. Figure 5 shows results for NDR and for comparison figure 6 shows results for the same cases but adopting the RD approach. There is no major difference between the two sets of results indicating that for this test case the use of returning or non-returning dampening is not significant. It is also apparent that the inclusion of twisting is again only a minor second order effect. The significant difference between the models is the stark contrast between the RSR and SSR models.

This difference is made even clearer in figures 7 and 8 where the drum is rotating at a speed above the critical speed (100 rpm or 126% of the critical speed). In the SSR cases the expected behaviour is observed where the drum has effectively become a centrifuge and the majority of particles travel around the edge of the drum. In the RSR case the particles still remain near the bottom of the drum, they do not travel around the edge and they all possess high rotational velocities. (The RSR approach is used in industrial simulations of rotating ball mills. However, industrial mills are typically designed with the inclusion of lifters or raised internal ledges on the drum. The presence of lifters will effectively mask the deficiencies of any friction model because the lifters will carry the particles up the side of the drum whereas in the smooth drum test case presented here only the frictional forces are providing the lifting effect.) Again, the significant difference between the models is the stark contrast between the RSR and SSR models, inclusion or non-inclusion of twisting and use of RD or NRD dampening models is a minor effect. As additional quantitative information figure 9 shows a histogram plot of radial velocities comparing the RSR and SSR models. The greater proportion of particles with much higher radial velocities in the RSR model, as compared to the SSR model, is very clear.

Figure 10 shows a graph of the summed total kinetic energy of all particles in the 60 rpm rotating drum simulation for all cases for returning dampening (RD), non-returning dampening (NRD), relative speed of rotation model (RSR), summed speed of rotation model (SSR) including or not including twisting effects. (NB the *RD_RSR_Twist* and *NRD_RSR_Twist* cases virtually overlie each other.) In these simulations there is an initial peak at about 0.2 seconds. This peak relates to the initial placing of the particles in the drum and their dropping and settling to the bottom of the drum. They then remain in a static pile until 2 seconds when the drum rotation is begun. The SSR model results then show periodic maxima and minima as particles move around the wall and periodically detach and fall downwards (figures 5 a and b). In contrast, most of the RSR models increase to a steady state summed kinetic energy as a result of the particles remaining near the base of the drum, rotating (as observed in figures 5 c and d), but not being carried around the wall. The inclusion or not of twist does affect the RSR results, this might be expected as the RSR model results in nearly all particles remaining close to the base of the drum with large amounts of in-contact particle rotation where twisting would be more significant. However, the RSR model is shown to not give the overall correct behaviour in the drum simulations.

To aid the reader the major differences between models are highlighted in figures 11-13. The difference in behaviour between SSR and RSR models is made clear in figure 11 that shows results for the NRD plus twisting simulations for SSR and RSR. For the NRD case the effect of twisting is seen to be minimal as highlighted by figure 12. Figure 13 shows the effect of using NRD or RD in the SSR case, where a difference is observed. Here the use of non-returning dampening lowers the overall kinetic energy of the system.

Figure 14 shows a graph of the summed total kinetic energy of all particles in the 100 rpm rotating drum simulation for all cases for returning dampening (RD), non-returning dampening (NRD), relative speed of rotation model (RSR), summed speed of rotation model (SSR) including or not including twisting effects. The stark difference between the SSR and RSR models is now made much clearer. Again, to aid the reader the major differences between models are highlighted in figures 15-17. The difference in behaviour between SSR and RSR models is very clear from figure 15 that shows results for the NRD plus twisting simulations for SSR and RSR. Figures 16 and 17 follow the same general trends as figures 12 and 13 but with a greater effect of twisting and lesser effect of dampening respectively at the higher drum rotational speeds.

In summary, the RSR model is not able to simulate the expected behaviour of a drum rotating at greater than the critical speed. While the use of NRD/RD and twisting/no-twisting do affect results, they are only second order effects in the simulations presented here.

Conclusions

When attempting to simulate large scale granular flows it is inevitable that numerical approximations will be required. For the case of blast furnace charging (figure 18) the use of the soft-sphere approximation allows full scale simulation to be achieved in timescales that are useful to industry. In reality the particles in a blast furnace are generally ‘spherical’ so the approximation is useful, provided that correct flow behaviour is achieved. The correct behaviour in soft sphere models is usually achieved by using suitable friction parameters. In this paper it is shown that the usual ‘relative speed of rotation’ approach for bending forces does not give results which are as good as a proposed ‘summed speed of rotation’ approach for a rotating drum simulation.

Acknowledgements

Thanks are extended to Tata Steel UK for their assistance throughout this project and for funding provided through the STRIP (Steel Training Research and Innovation Partnership) scheme. STRIP has been made possible by the EU Convergence European Social Fund through the Welsh Government.

References

[1] M.A.J. Holmes, S.G.R. Brown, DEM Prediction Of Burden Distribution Patterns In A Blast Furnace Bell-Less Top Charging System, 6th International Conference on

Discrete Element Methods (DEM6), 5-6 August 2013, Colorado School of Mines, Colorado, USA.
[2] I.F. Kurunov, Efficiency of using different types of charging apparatuses on blast furnaces, Metallurgist, 53 (2009) 661-671.
[3] A. Adema, Y. Yang, R. Boom, Coupled DEM – CFD Modelling of the ironmaking blast furnace, Seventh International Conference on CFD in the Minerals and Process Industries, CSIRO Australia (2009) 1-6.
[4] Y. Yu, H. Saxén, Experimental and DEM study of segregation of ternary size particles in a blast furnace top bunker model, Chemical Engineering Science 65 (2010) 5237–5250.
[5] H. Mio, S. Matsuzaki, K. Kunitomo, J. Hidaka, Analysis of particle charging behaviour via rotating chute of blast furnace by using discrete element method, The Fifth International Conference on Discrete Element Methods, QMUL, London (2010) 496- 501.
[6] R.D. Mindlin, Compliance of Elastic Bodies in Contact, Journal of Applied Mechanics, 16 (1949) 259-268.
[7] Y.C. Zhou, B.D. Wright, R.Y. Yang, B.H. Xu, A.B. Yu, Rolling friction in the dynamic simulation of sandpile formation, Physica A 269 (1999) 536-553.
[8] Y.C. Zhou, B.H. Xu, A.B. Yu, P. Zulli, An experimental and numerical study of the angle of repose of coarse spheres, Powder Technology 125 (2002) 45– 54.
[9] J. Liu, J. Zhou, Numerical study on sandpile formation of granular materials with different grain size distributions, Geotechnical Engineering for Disaster Mitigation and Rehabilitation, Science Press Beijing and Springer-Verlag GmbH Berlin Heidelberg, Part 4, (2008) 374-380.
[10] J. Ai, J.F. Chen, J.M. Rotter, J.Y. Ooi, Assessment of rolling resistance models in discrete element simulations, Powder Technology 206 (2011) 269–282.
[11] Y. Wang, A new algorithm to model the dynamics of 3-D bonded rigid bodies with rotations, Acta Geotechnica 4 (2009) 117-127.
[12] M.R. Kuhn, K. Bagi, Contact rolling and deformation in granular media, International Journal of Solids and Structures 41 (2004) 5793–5820.
[13] K.M. Khan, G. Bushell, Comment on ‘‘Rolling friction in the dynamic simulation of sandpile formation’’, Physica A 352 (2005) 522–524.
[14] P.A. Cundall, O.D.L. Strack, A discrete numerical model for granular assemblies, Géotechnique, 29 (1979) 47–65.
[15] M.A.J. Holmes, ‘A Numerical Simulation of Particulate Distribution of the Blast Furnace Raw Materials Burden through the Paul Worth Bell-Less Top Apparatus’, Engineering Doctorate Thesis, Swansea University, UK, 2015.

Figure Captions

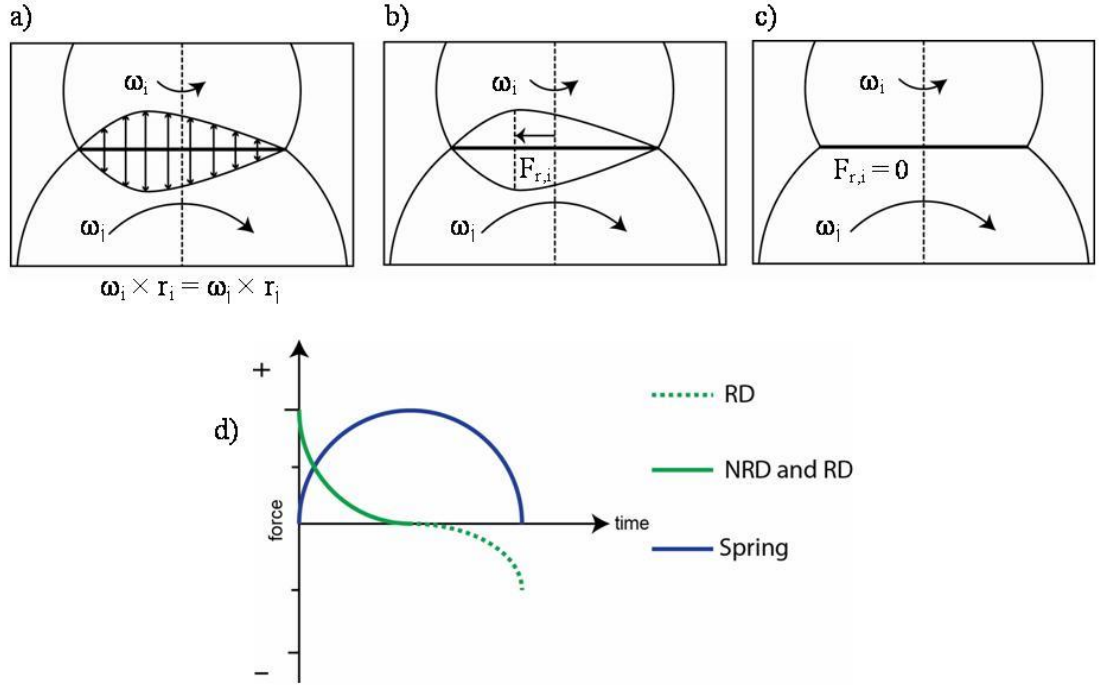

Figure 1. (a) Force distribution in two spheres in contact with equal surface velocities. (b) Schematic of rolling friction arising from the SSR formulation. (c) Zero rolling friction arising from the RSR formulation [13]. (d) Two different dampening models and the spring force arising from a collision.

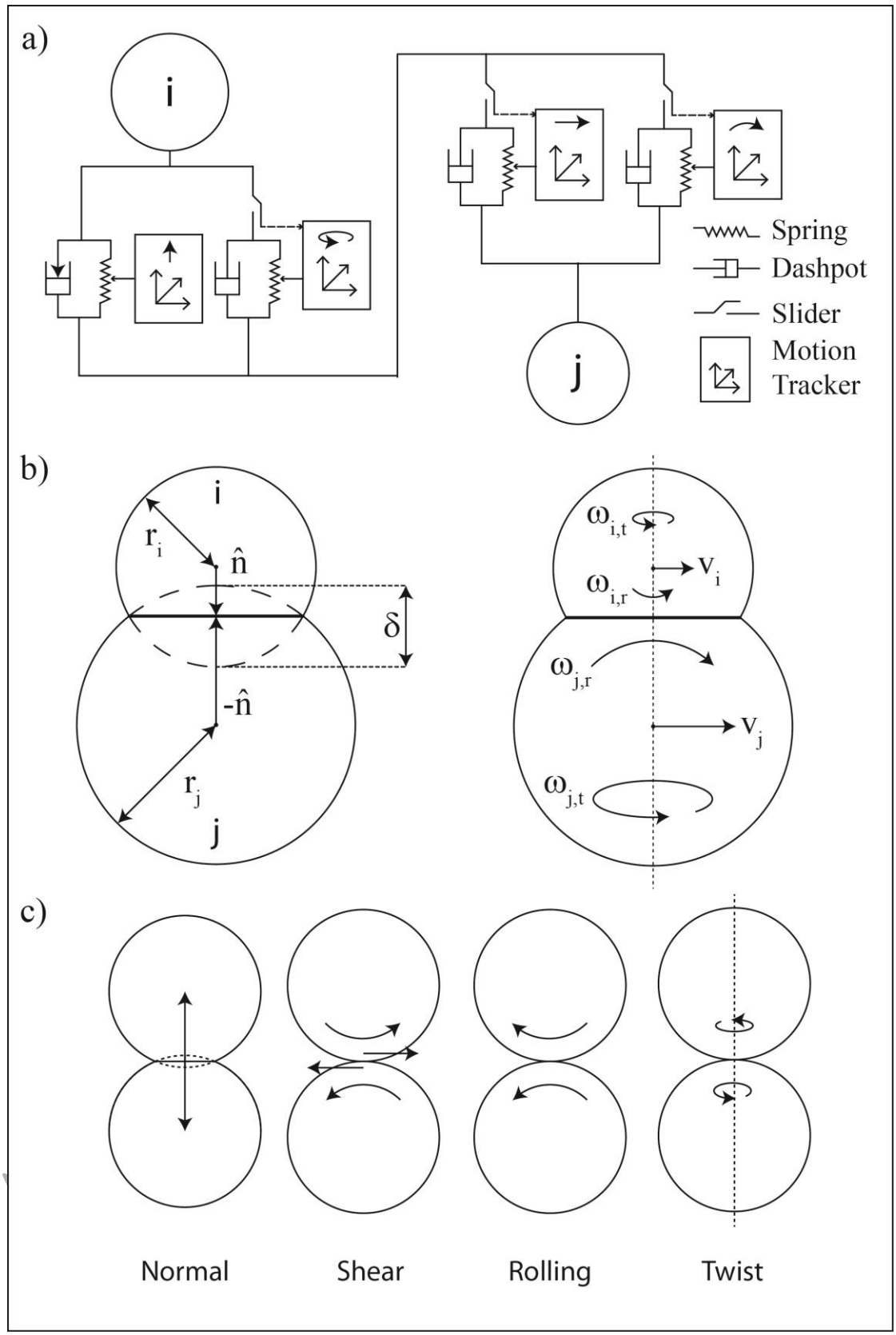

Figure 2. (a) The force model (top). (b) Distance and velocity definitions. (c) Degrees of freedom in the model.

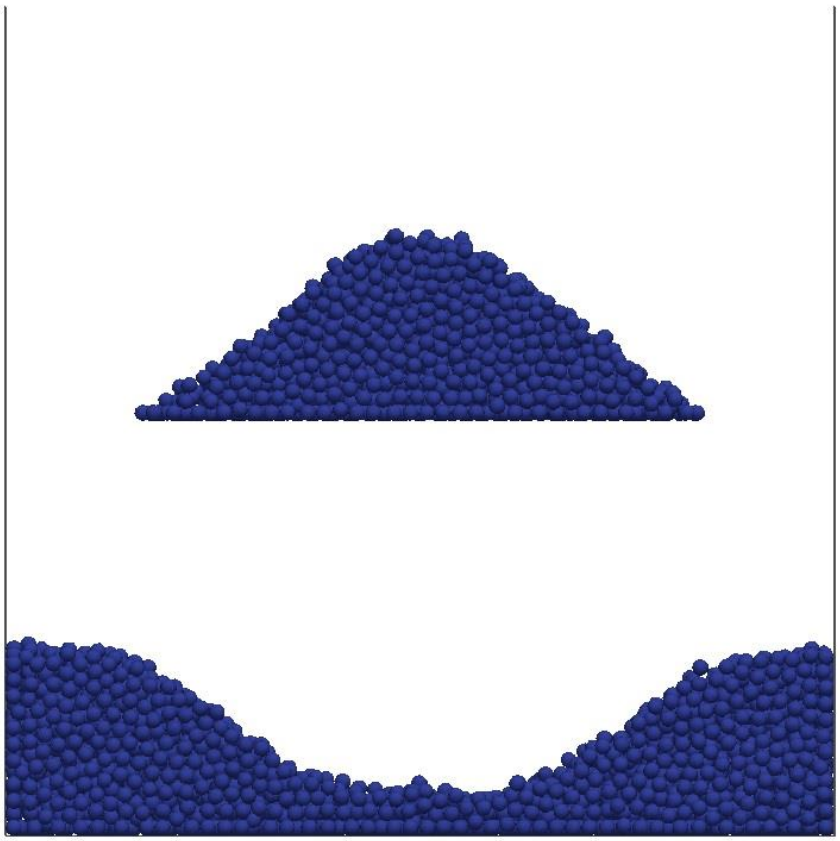

(a)

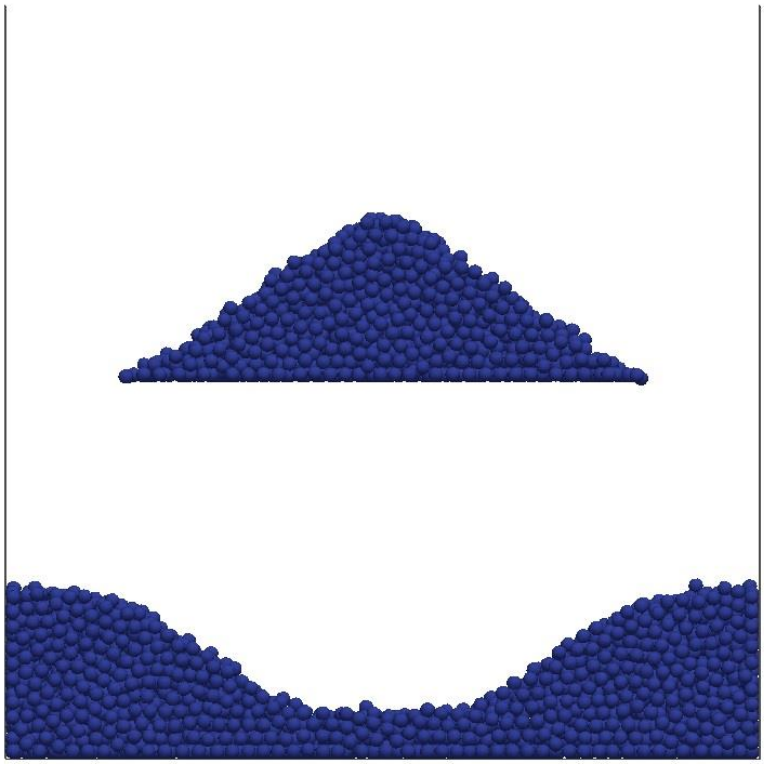

(b)

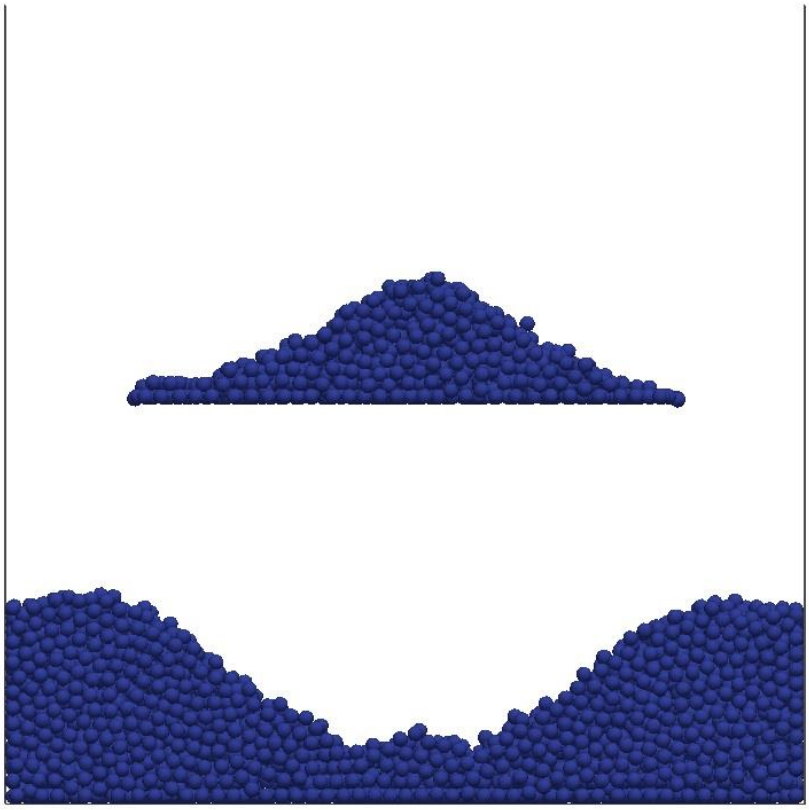

(c)

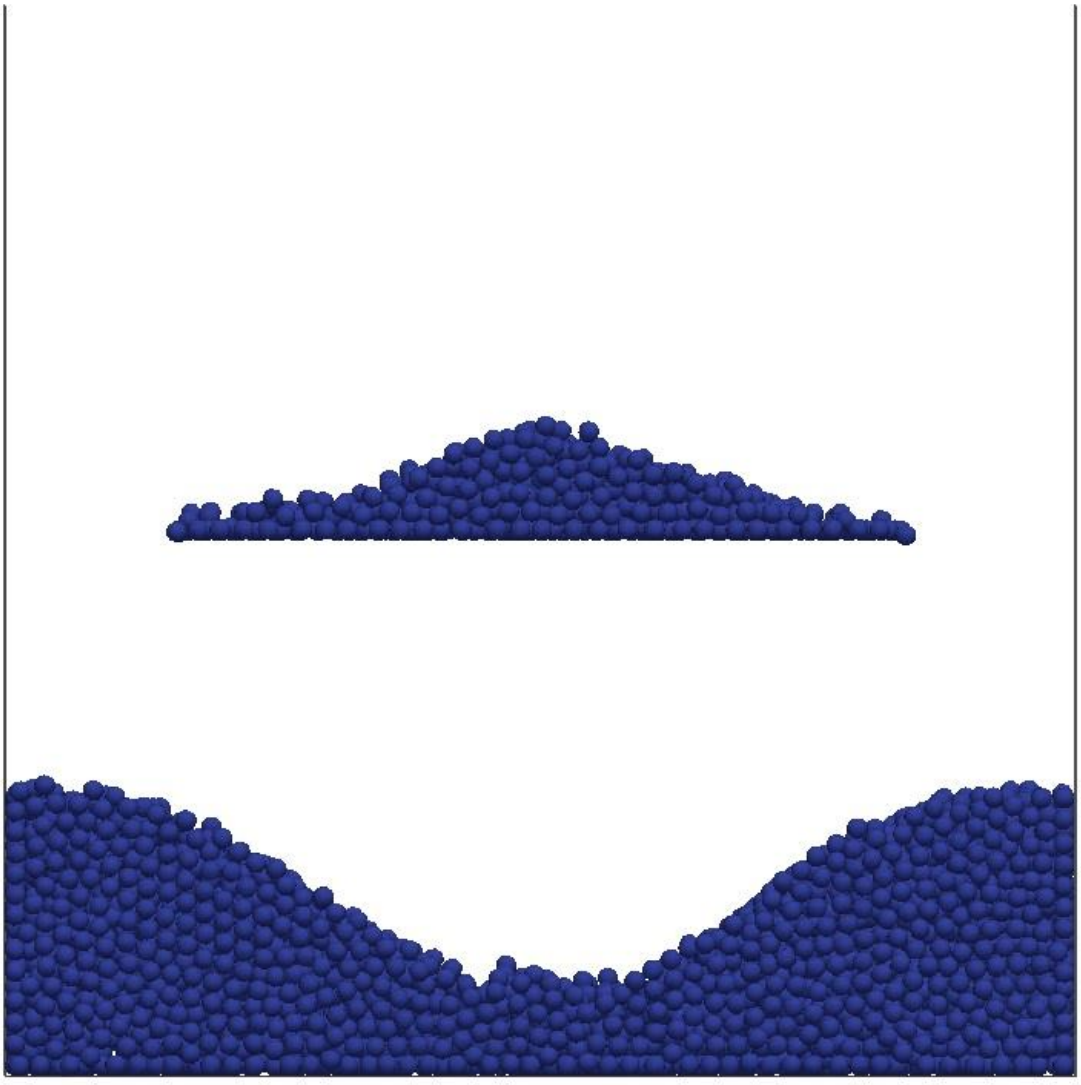

(d)

Figure 3. Results of simulations for the ledge test problem (Zhou et al 2002) using summed and relative speeds of rotation to calculate bending friction. These two cases have also been simulated with and without the inclusion of twisting. A non-returning dampener has been used in all cases. (a) NRD SSR Twist, (b) NRD SSR No Twist, (c) NRD RSR Twist, (d) NRD RSR No Twist.

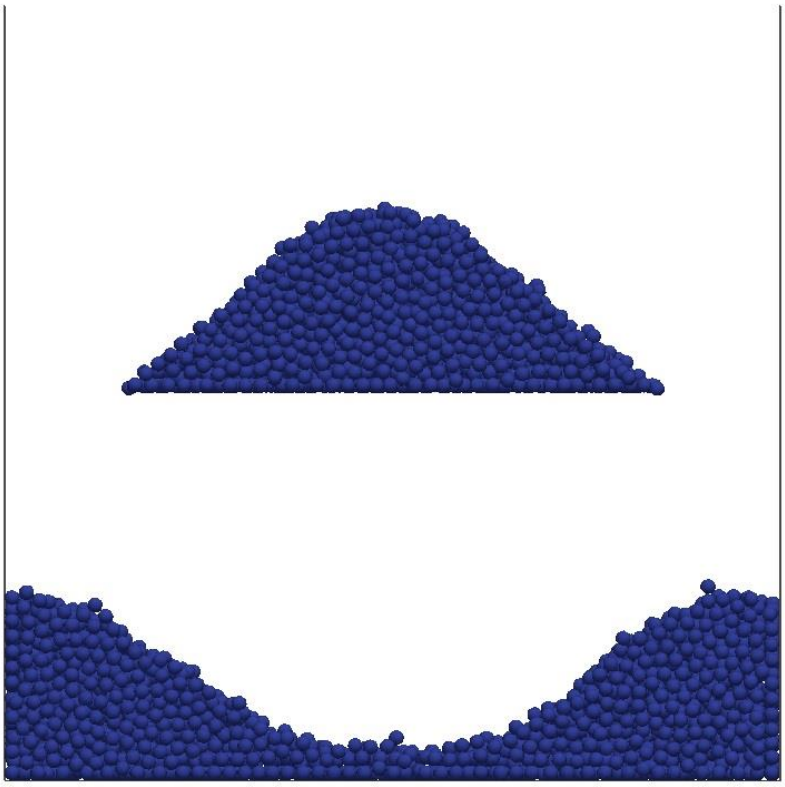

(a)

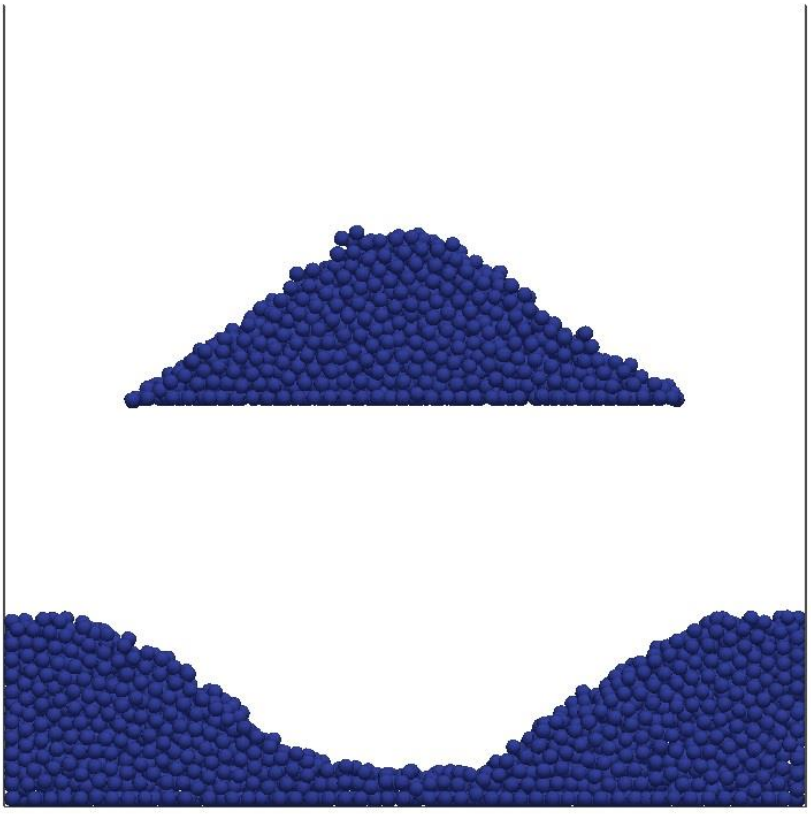

(b)

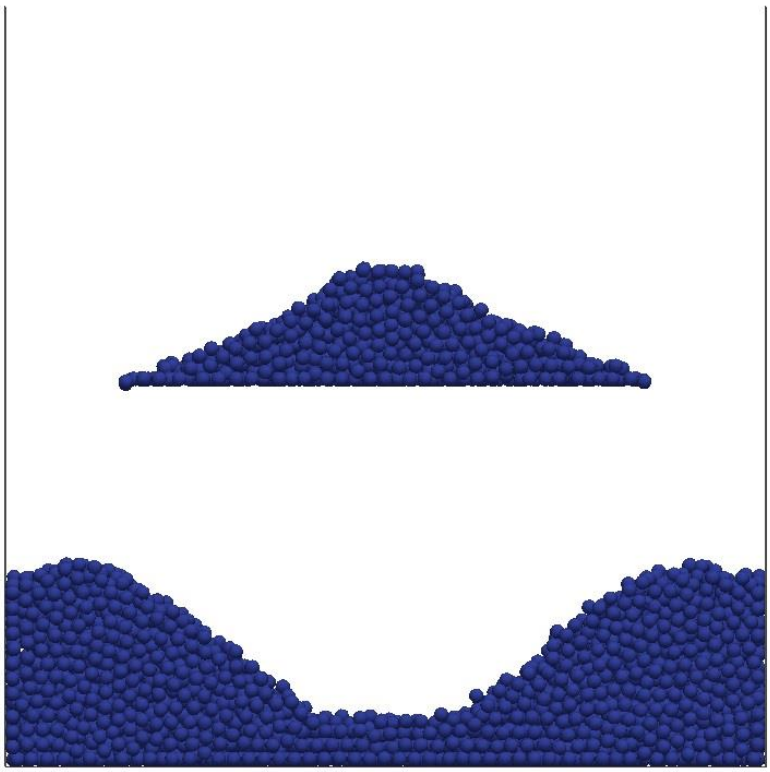

(c)

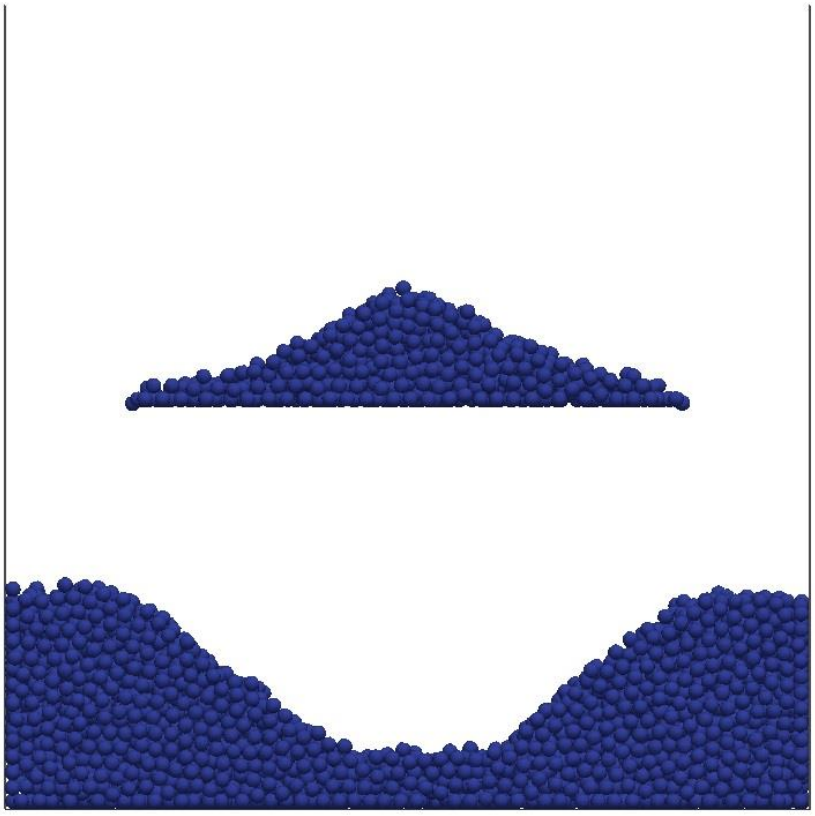

(d)

Figure 4. Results of simulations for the ledge test problem (Zhou et al 2002) using summed and relative speeds of rotation to calculate bending friction. These two cases have also been simulated with and without the inclusion of twisting. A returning

dampener has been used in all cases. (a) RD SSR Twist, (b) RD SSR No Twist, (c) RD RSR Twist, (d) RD RSR No Twist, (e) RD SSR Twist (coefficients/2).

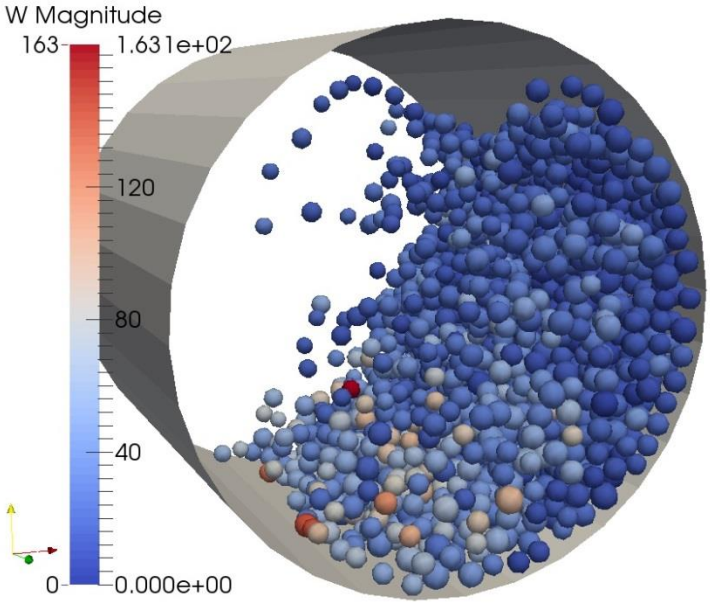

(a)

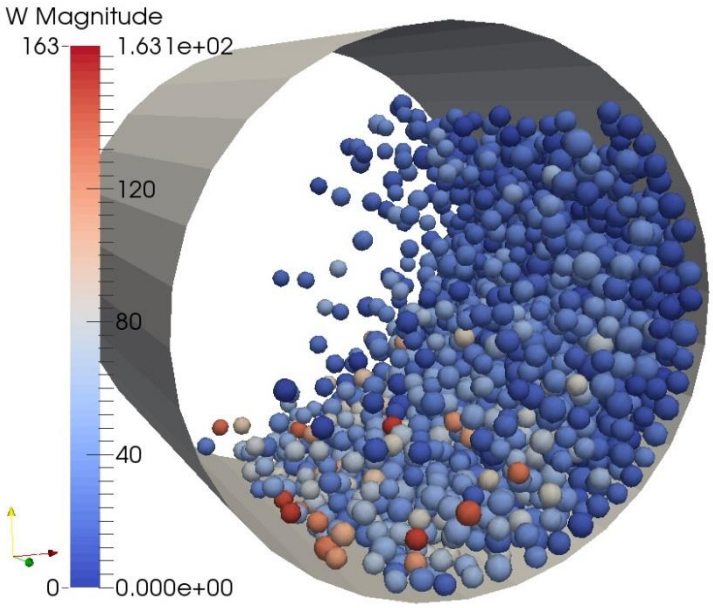

(b)

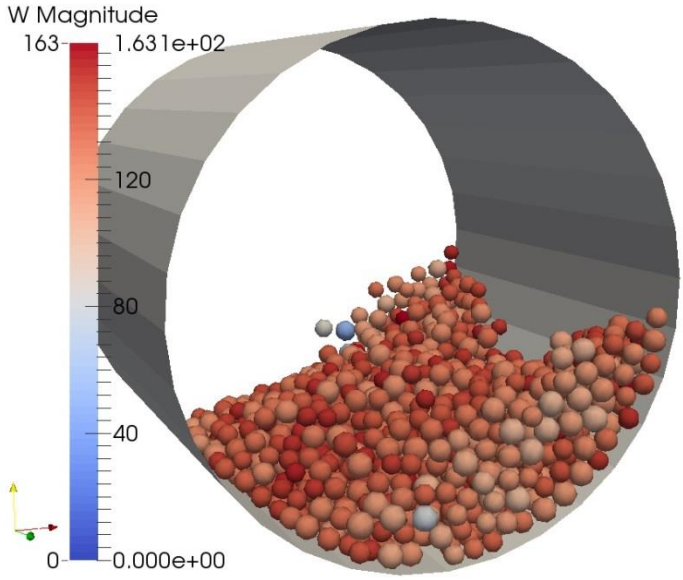

(c)

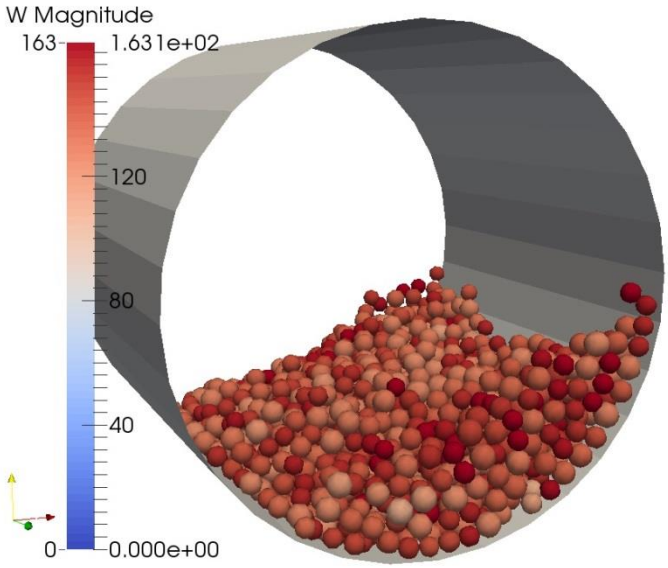

(d)

Figure 5. Rotating drum simulations at 70% of the critical speed (60 rpm) for two different bending friction approaches using summed and relative speeds of rotation to calculate bending friction. These two cases have also been simulated with and without the inclusion of twisting. A non-returning dampener has been used in all cases. (a) NRD SSR Twist, (b) NRD SSR No Twist, (c) NRD RSR Twist, (d) NRD RSR No Twist. The legend shows W, the magnitude of rotational velocity in radians/s.

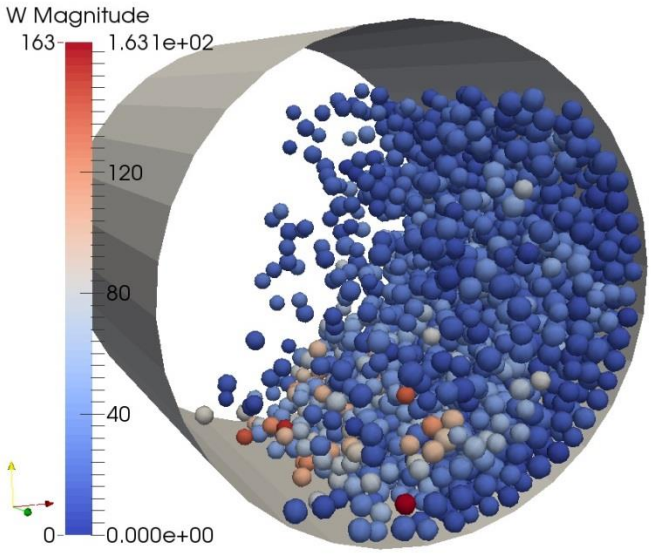

(a)

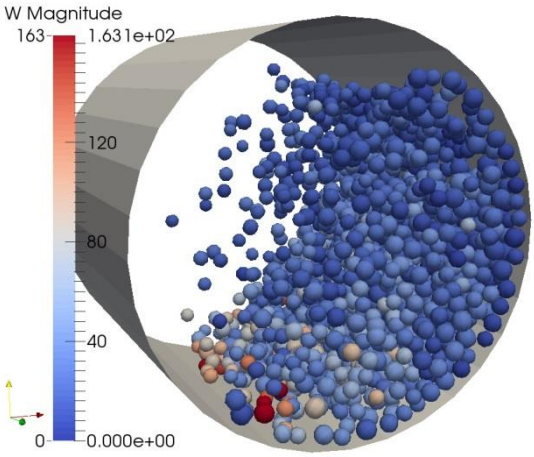

(b)

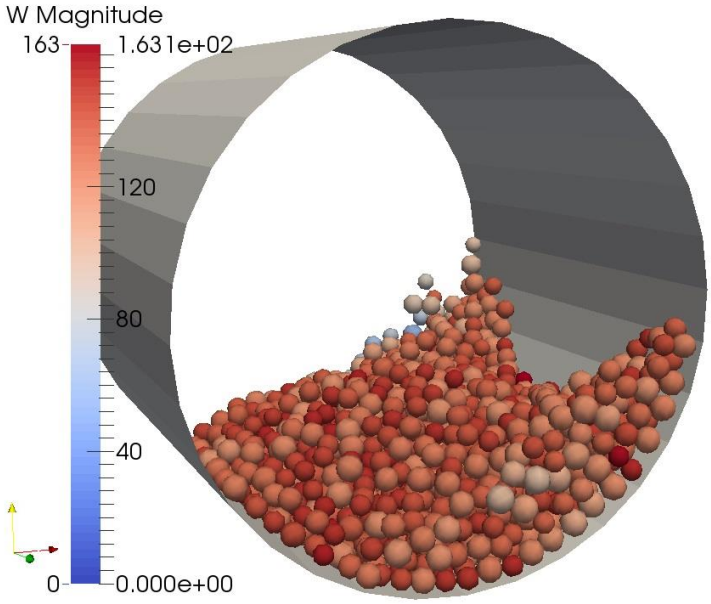

(c)

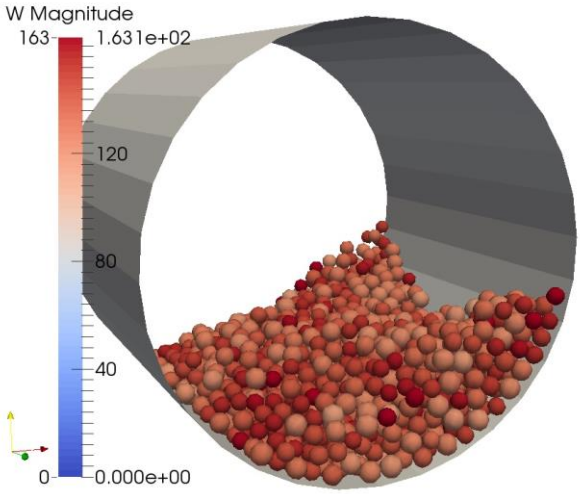

(d)

Figure 6. Rotating drum simulations at 70% of the critical speed (60 rpm) for two different bending friction approaches using summed and relative speeds of rotation to calculate bending friction. These two cases have also been simulated with and without the inclusion of twisting. A returning dampener has been used in all cases. (a) RD SSR twist, (b) RD SSR No twist, (c) RD RSR twist, (d) RD RSR No twist. The legend shows W, the magnitude of rotational velocity in radians/s.

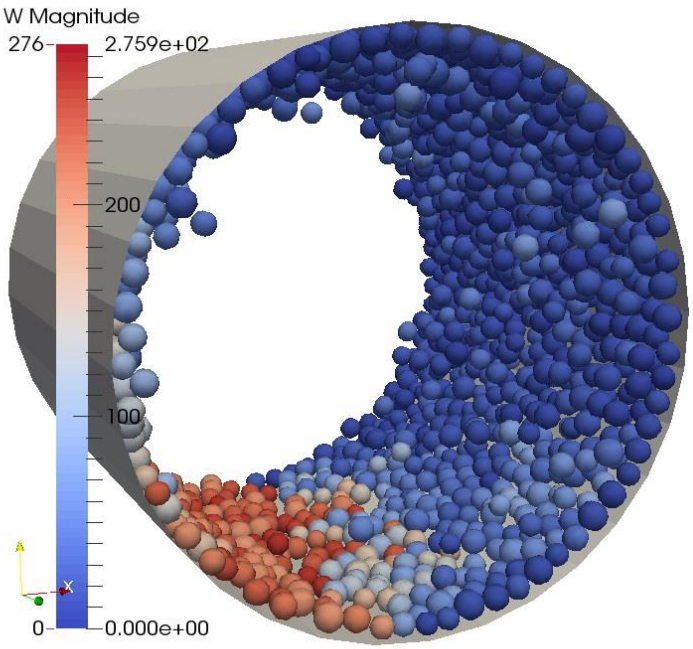
W Magnitude
276
2.759e+02
200
100
0
0.000e+00

(a)

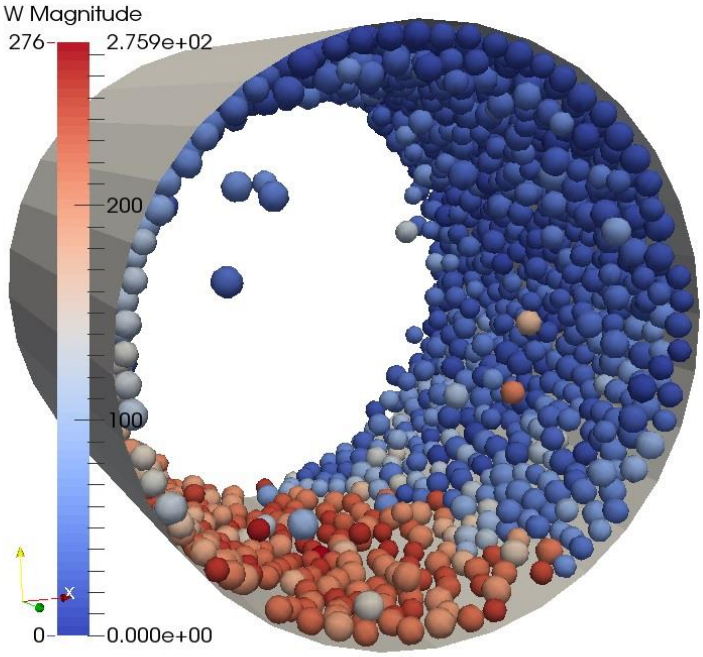
W Magnitude
276
2.759e+02
200
100
0
0.000e+00

(b)

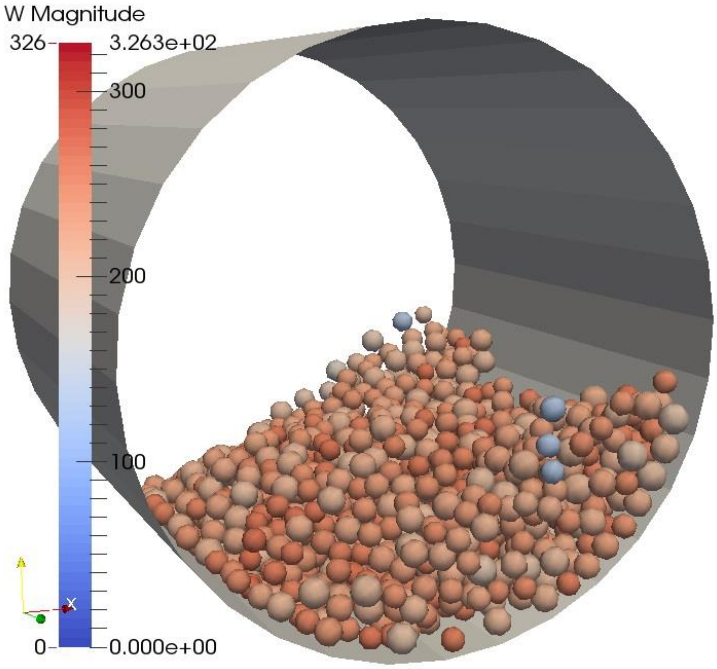

(c)

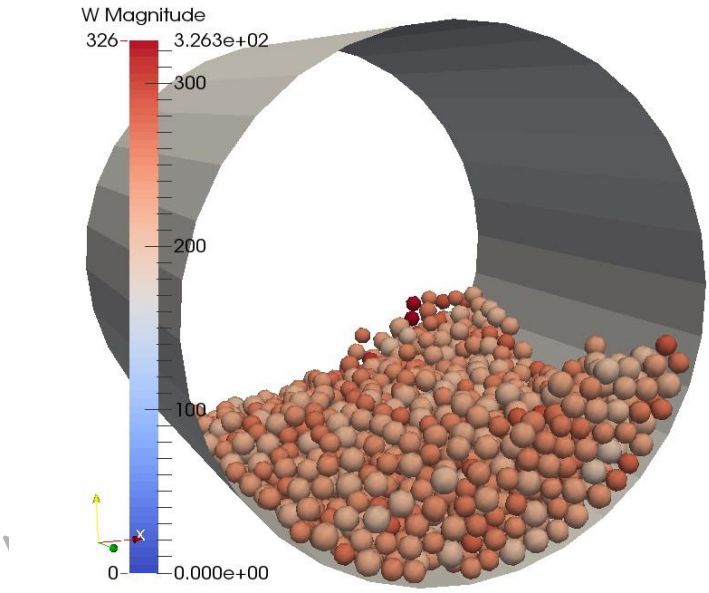

(d)

Figure 7. Rotating drum simulations at 126% of the critical speed (100 rpm) for two different bending friction approaches using summed and relative speeds of rotation to calculate bending friction. These two cases have also been simulated with and without the inclusion of twisting. A non-returning dampener has been used in all cases. (a) NRD SSR twist, (b) NRD SSR No twist, (c) NRD RSR twist, (d) NRD RSR No twist. The legend shows W, the magnitude of rotational velocity in radians/s.

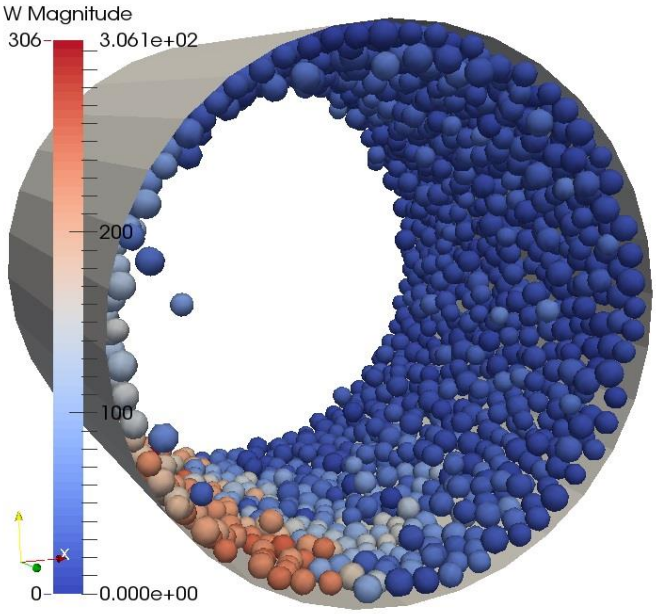

(a)

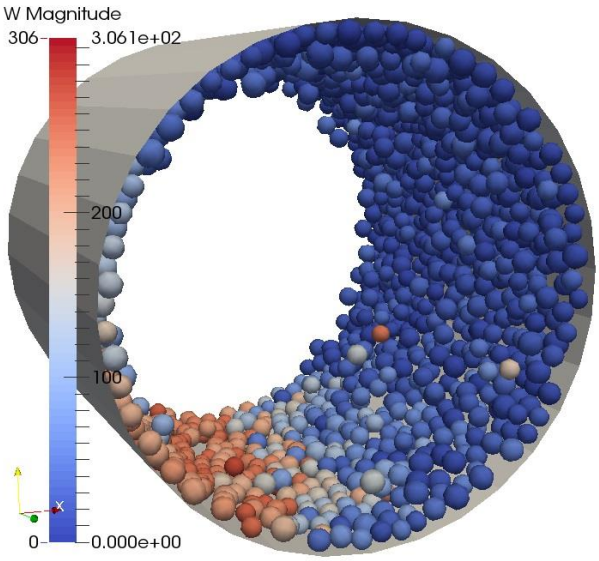

(b)

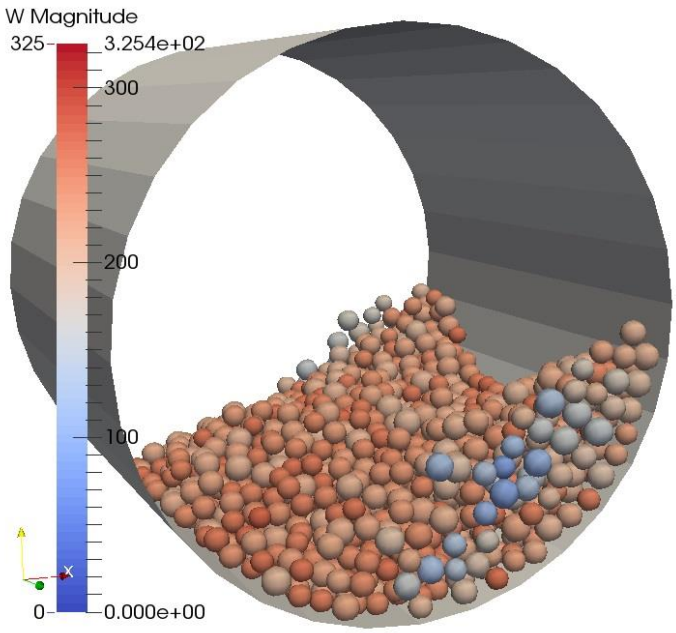

(c)

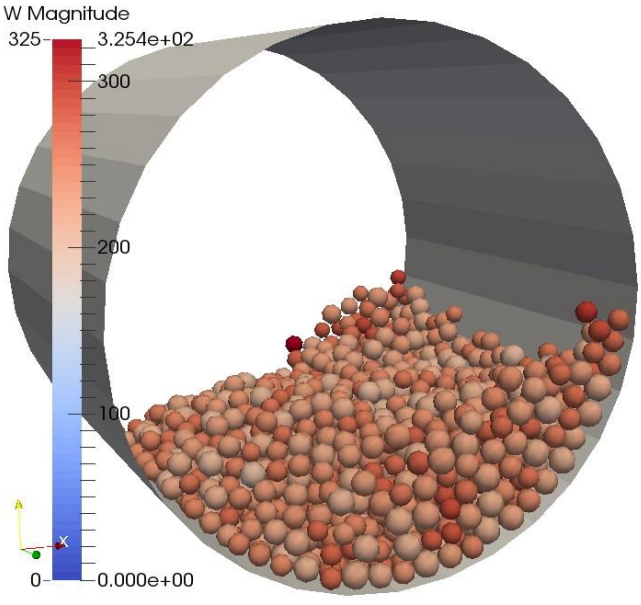

(d)

Figure 8. Rotating drum simulations at 126% of the critical speed (100 rpm) for two different bending friction approaches using summed and relative speeds of rotation to calculate bending friction. These two cases have also been simulated with and without the inclusion of twisting. A returning dampener has been used in all cases. (a) RD SSR twist, (b) RD SSR No twist, (c) RD RSR twist, (d) RD RSR No twist. The legend shows W, the magnitude of rotational velocity in radians/s.

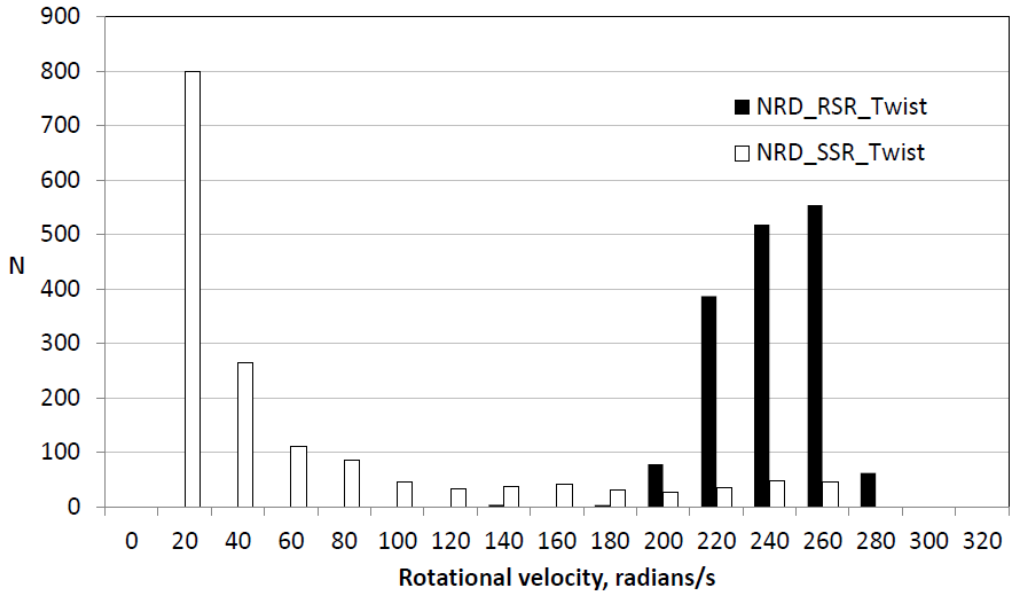

Figure 9. Histogram plot showing distribution of radial velocities for the NRD SSR twist and NRD RSR twist cases; corresponding to simulation results shown in figures 7 a and b respectively.

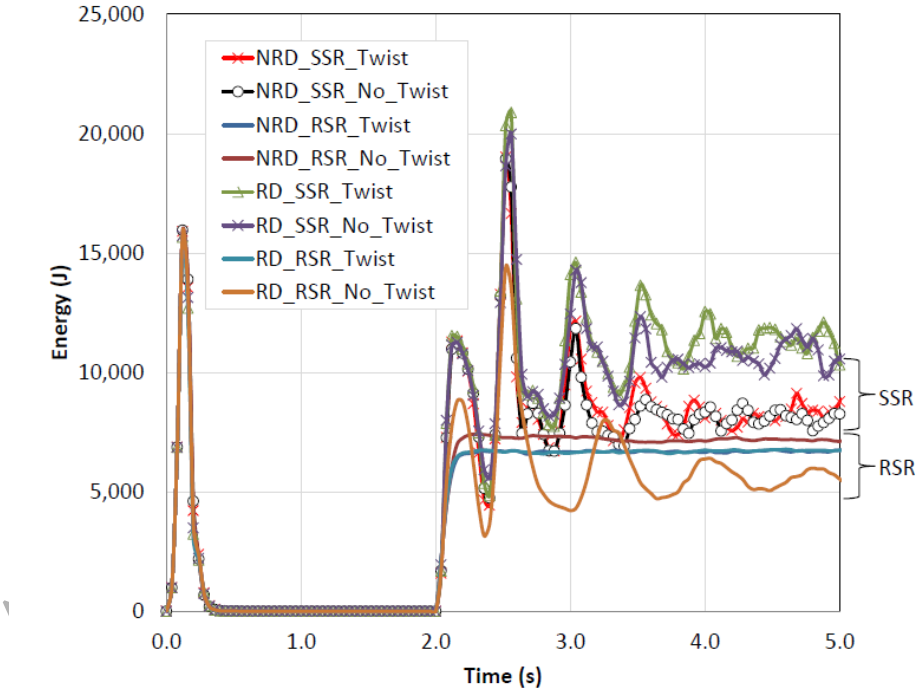

Figure 10. Summed total kinetic energy of all particles in 60 rpm drum simulation for all simulated cases with returning dampening (RD), non-returning dampening (NRD), relative speed of rotation model (RSR), summed speed of rotation model (SSR) including or not including twisting effects.

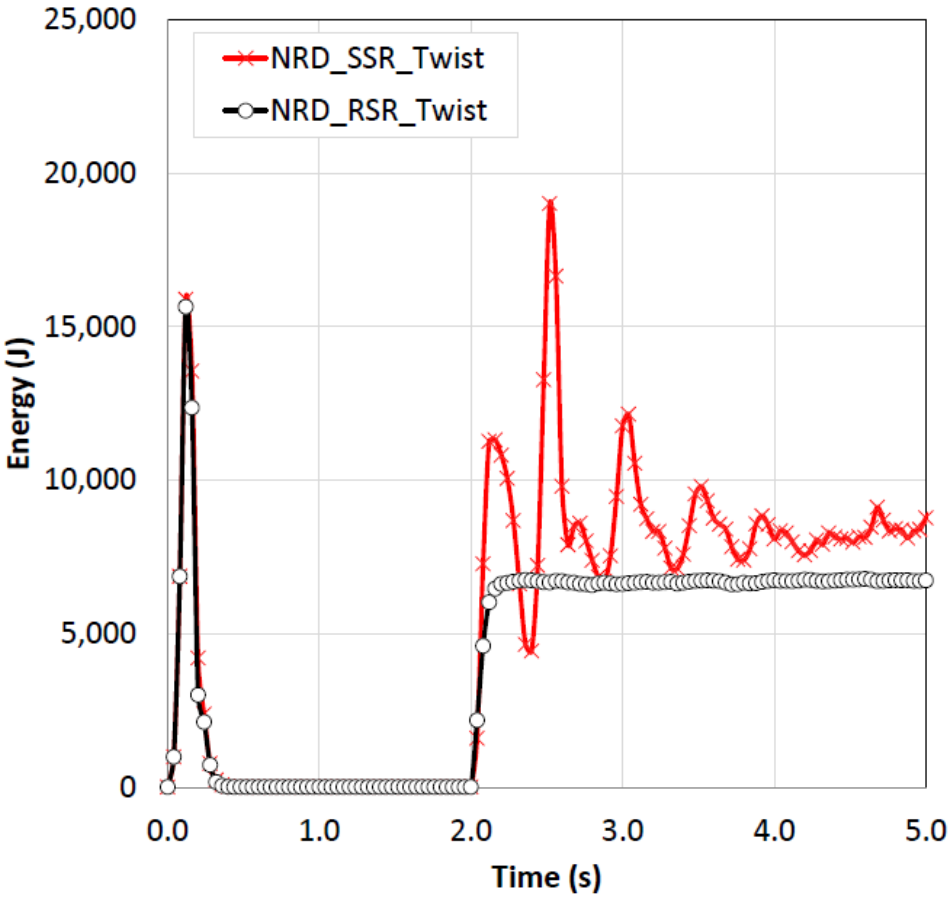

Figure 11. Summed total kinetic energy of all particles in 60 rpm drum simulation for non-returning dampening (NRD) including twisting effects comparing the relative speed of rotation model (RSR) to the summed speed of rotation model (SSR).

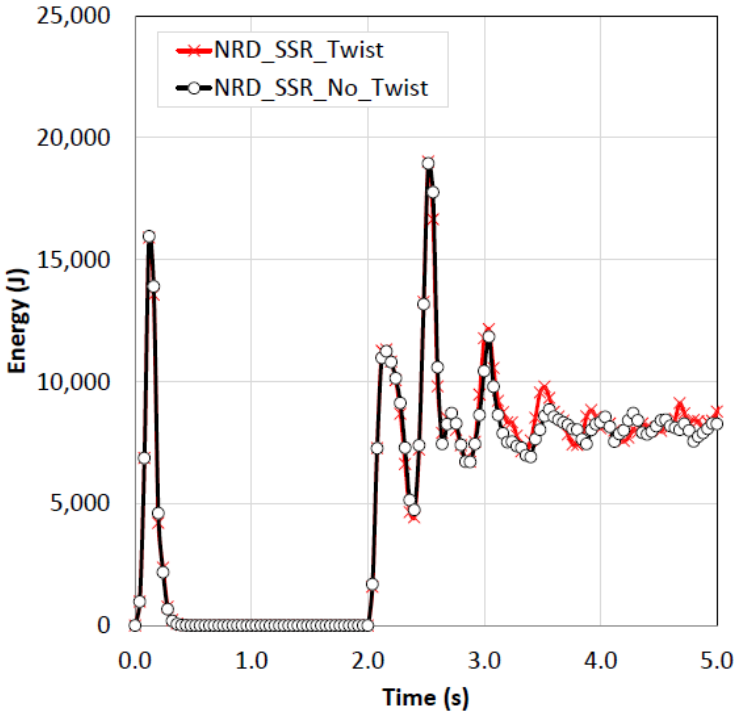

Figure 12. Summed total kinetic energy of all particles in 60 rpm drum simulation for non-returning dampening (NRD) and the summed speed of rotation model (SSR) comparing the inclusion or omission of twisting effects.

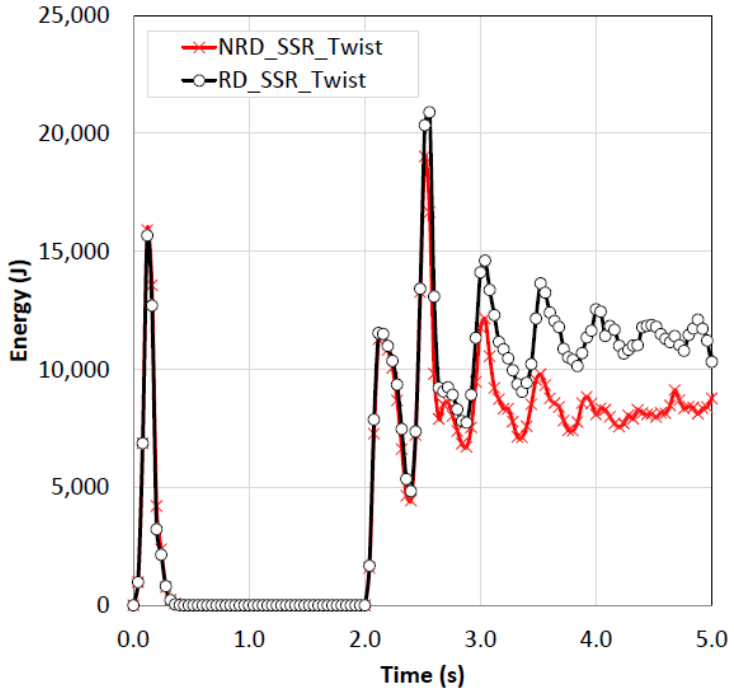

Figure 13. Summed total kinetic energy of all particles in 60 rpm drum simulation for the summed speed of rotation model (SSR) including twisting effects, comparing the use of non-returning dampening (NRD) to returning dampening (RD).

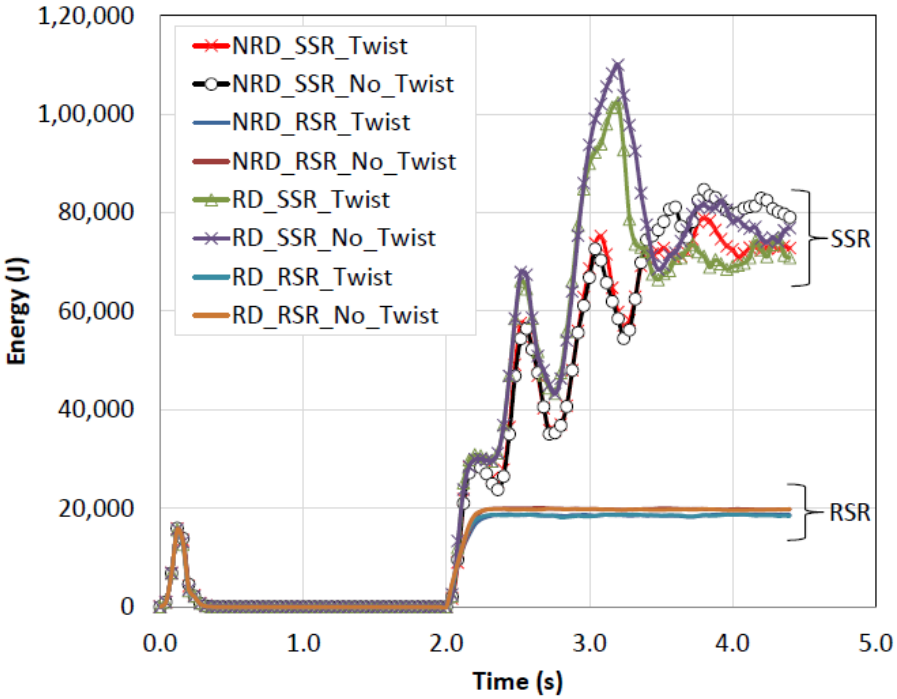

Figure 14. Summed total kinetic energy of all particles in 100 rpm drum simulation for all simulated cases with returning dampening (RD), non-returning dampening (NRD), relative speed of rotation model (RSR), summed speed of rotation model (SSR) including or not including twisting effects.

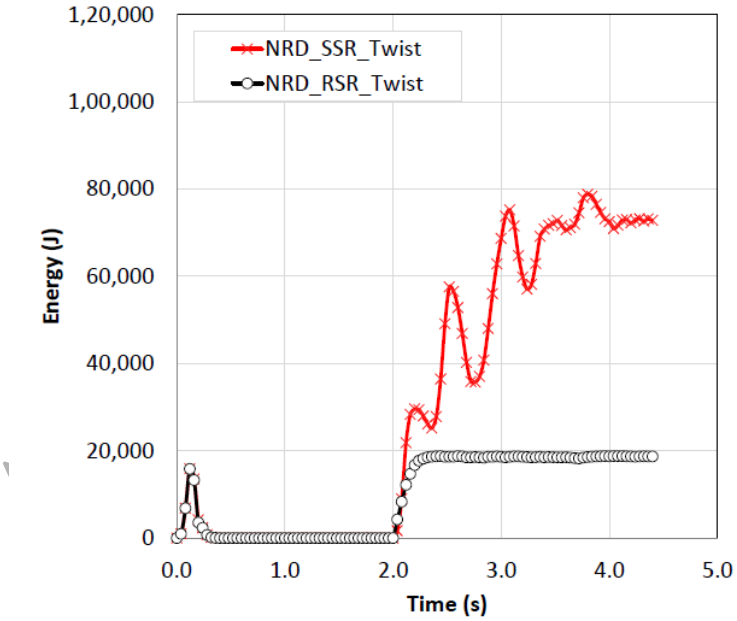

Figure 15. Summed total kinetic energy of all particles in 100 rpm drum simulation for non-returning dampening (NRD) including twisting effects comparing the relative speed of rotation model (RSR) to the summed speed of rotation model (SSR).

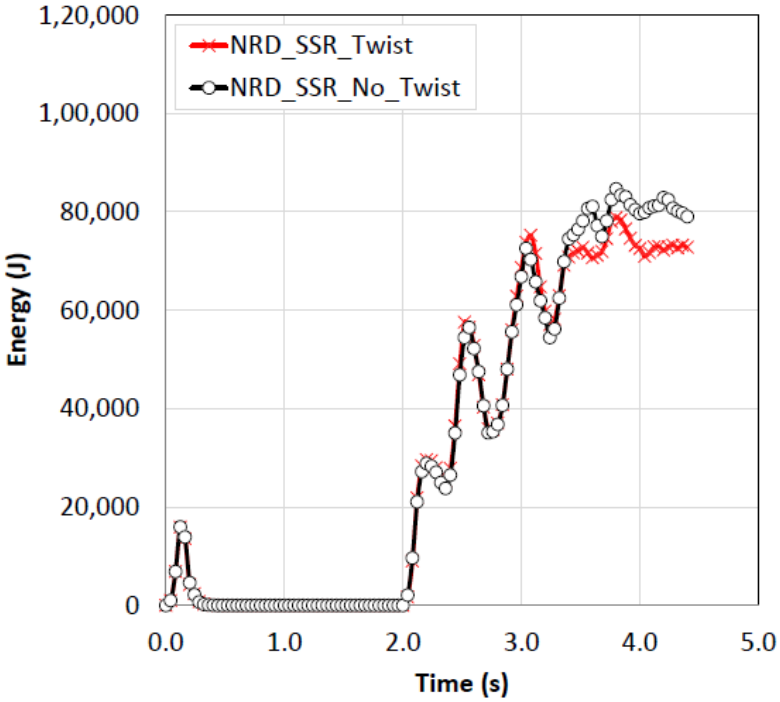

Figure 16. Summed total kinetic energy of all particles in 100 rpm drum simulation for non-returning dampening (NRD) and the summed speed of rotation model (SSR) comparing the inclusion or omission of twisting effects.

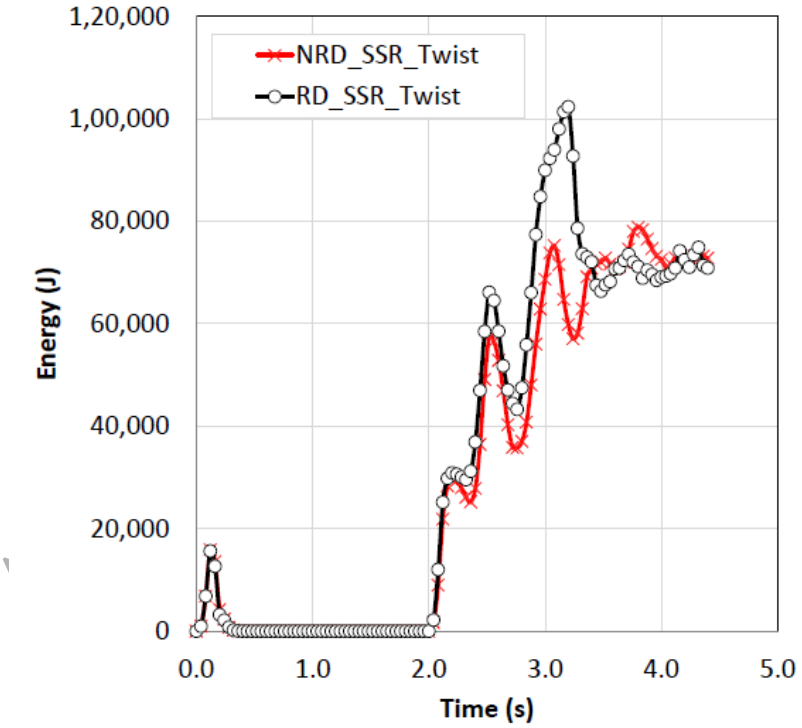

Figure 17. Summed total kinetic energy of all particles in 100 rpm drum simulation for the summed speed of rotation model (SSR) including twisting effects, comparing the use of non-returning dampening (NRD) to returning dampening (RD).

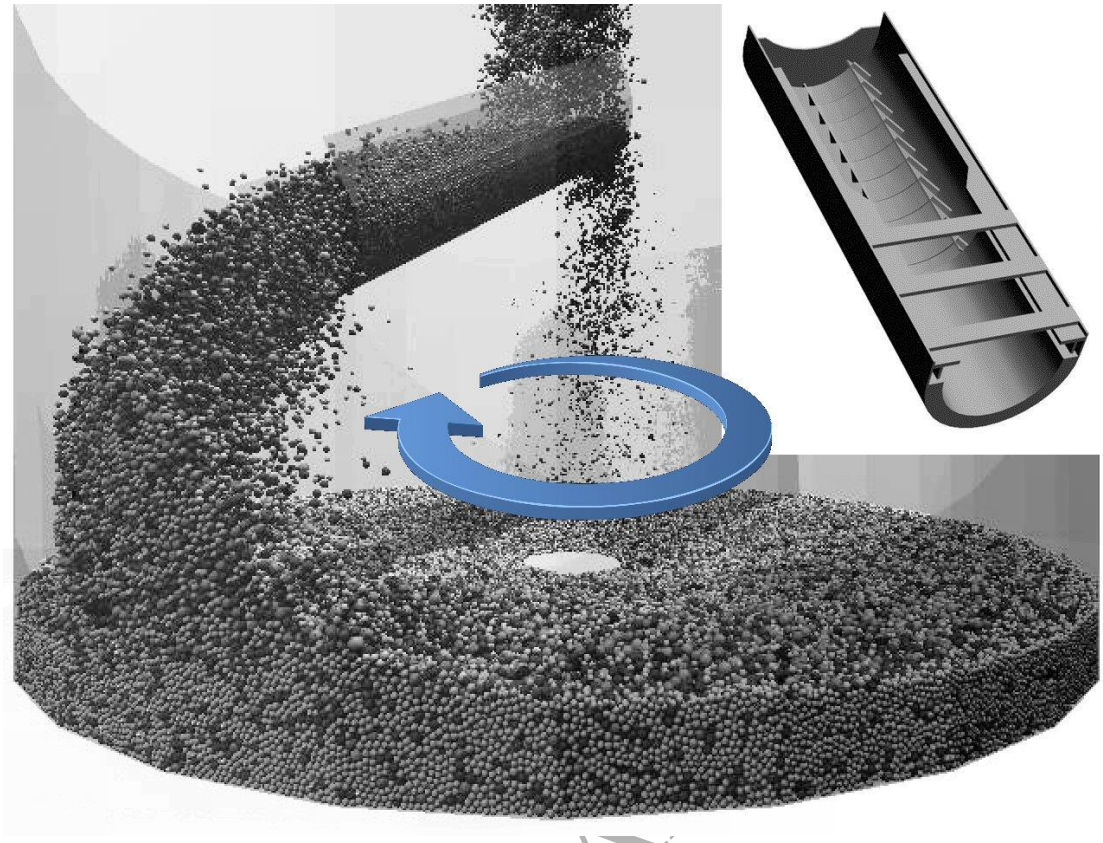

Figure 18. Full scale DEM simulation of blast furnace charging showing the burden being distributed by chute rotating in the direction of the arrow. The detailed chute design is shown in the upper right.

Table 1. Simulation parameters and run time information. Where (pp) is particle-particle and (wp) is wall-particle interaction. Random particle size distributions were generated with a uniform distribution. Computer specification: Intel W3680 @3.33GHz, 24GB DDR3 RAM, Windows 7.

Type	***Ledge test***	***Drum test***	***Units***
Fixed time increment, dt	1.00E-06	1.00E-05	s
Spring constant, k_s	64000	16000	$kg \cdot m \cdot s^{-2}$
Coefficient of restitution, η_n	0.02	0.02	
Shear constant, k_s	24615	6154	$kg \cdot m \cdot s^{-2}$
Shear friction coefficient (pp), μ_s	0.7	0.8	
Shear friction coefficient (wp), μ_s	0.4	0.8	
Rolling friction coefficient (pp), μ_r	0.1	0.2	
Rolling friction coefficient (wp), μ_r	0.05	0.4	
Twisting friction coefficient (pp), μ_t	0.1	0.2	
Twisting friction coefficient (wp), μ_t	0.05	0.4	
Rotational dampening coefficient, η_r	1.5	1.5	
Maximum particle radius, r	0.005	0.008	m
Minimum particle radius, r	0.003	0.006	m
Density	2500	4500	$kg \cdot m^{-3}$
Total mass of particles	1.131	10.13	kg
Number of particles created	~1670	~1606	

	Ledge test	**drum 100 rpm**	**drum 60 rpm**	
Simulation time	60	4.4	6	s
Run time	19.33	0.23	0.40	hours